

Cite this: *Chem. Sci.*, 2019, 10, 1626

All publication charges for this article have been paid for by the Royal Society of Chemistry

# Rare “Janus”-faced $\{\text{Fe}^{\text{II}}\}$ single-molecule magnet exhibiting intramolecular ferromagnetic interactions†

Dimitris I. Alexandropoulos,<sup>a</sup> Kuduva R. Vignesh,<sup>a</sup> Theocharis C. Stamatatos<sup>\*b</sup> and Kim R. Dunbar<sup>\*a</sup>

A rare  $[\text{Fe}^{\text{II}}(\text{N}_3)_{12}(\text{MeCN})_{12}](\text{ClO}_4)_2$  disk-like single-molecule magnet (SMM) exclusively bridged by end-on azides with a spin ground state of  $S = 14$  was prepared by the reaction of a divalent  $\text{Fe}^{\text{II}}$  precursor with  $\text{Me}_3\text{SiN}_3$  under basic conditions. AC magnetic susceptibility studies revealed unusual, “Janus”-faced SMM behavior for the dried and pristine forms of the  $\{\text{Fe}^{\text{II}}\}$  compound attributed to solvation/de-solvation effects of the coordinated MeCN ligands which leads to alterations in the crystal field and symmetry of the metal ions. DFT calculations confirmed the ferromagnetic nature of the interactions between the  $\text{Fe}^{\text{II}}$  spin carriers with the zero-field splitting parameters  $D = -0.2323 \text{ cm}^{-1}$  and  $E/D = 0.027$ . The results have important implications for the future study of single-molecule magnets incorporating volatile solvent molecules in the first coordination sphere of the metal ions and their effect on the relaxation dynamics.

Received 3rd October 2018  
Accepted 3rd November 2018

DOI: 10.1039/c8sc04384a

rsc.li/chemical-science

## Introduction

Single-molecule magnets (SMMs) are coordination compounds that exhibit slow relaxation of their magnetization at the molecular level,<sup>1</sup> a property that renders them suitable candidates for emerging technologies including high density data storage,<sup>2</sup> molecular electronic devices,<sup>3</sup> and quantum computation.<sup>4</sup> In the quest for strongly-coupled polynuclear SMMs with enhanced properties, one of the most difficult challenges to overcome is the combination of a large spin ground state ( $S$ ) with a large and negative zero-field splitting parameter, as defined by the axial parameter,  $D$ .<sup>1</sup> To this end, bridging ligands have played a special role in not only fostering ferromagnetic exchange interactions between the metal ions they bridge, through either a superexchange<sup>5</sup> or direct mechanism,<sup>6</sup> but also in controlling the orientation of the magnetic anisotropy axes<sup>7</sup> and stabilizing microstates with the largest spin and orbital angular momenta.<sup>8</sup>

In recent years 4f metal containing molecules have attracted considerable interest in the SMM field vis-à-vis enhancing the magnetization dynamics (*i.e.*, large energy barriers and

blocking temperatures).<sup>9</sup> The progress in this area notwithstanding, there are limitations including effective quantum tunneling of the magnetization at zero field and weak-to-negligible magnetic exchange interactions due to the efficient shielding of the 4f orbitals by the outer 5s and 5p-orbitals.<sup>10</sup> Given these issues, 3d metal based SMMs of oligo- and polynuclear complexes are still worth pursuing.<sup>11</sup>

The syntheses of transition metal molecules with interesting magnetic properties often relies on self-assembly reactions between 3d-metal precursors and organic chelating/bridging ligands.<sup>11b</sup> This strategy has afforded a plethora of SMMs with modest barriers but also some of the most spectacular and well-known SMMs to date including the ubiquitous  $\{\text{Mn}_{12}\}$ -carboxylate<sup>12</sup> and  $\{\text{Mn}_6\}$ -oximate complexes,<sup>13</sup> and, recently, a nano-sized  $\{\text{Mn}_{31}\}$  cluster<sup>14</sup> and a low-coordinate  $\{\text{Co}_4\}$  compound,<sup>15</sup> all with high energy barriers and blocking temperatures. Unlike Mn compounds, Fe-based SMMs are scarce in the literature. Only a few trivalent  $\text{Fe}^{\text{III}}$  SMMs<sup>16</sup> have been reported to date and divalent  $\text{Fe}^{\text{II}}$  examples are limited to three examples, *viz.*, an  $\{\text{Fe}_2^{\text{II}}\}$ ,<sup>17</sup> a family of  $\{\text{Fe}_4^{\text{II}}\}$  cubanes,<sup>18</sup> and a nonanuclear  $\{\text{Fe}_9^{\text{II}}\}$  compound.<sup>19</sup> Although organic bridging ligands assist in the thermodynamic stability, solubility, and crystallinity of 0-D compounds, their presence as neutral linkers often limits the magnetic properties and dynamics of SMMs, leading to competing magnetic interactions, moderate-to-weak magnetic couplings, and low-lying excited states, among others.<sup>11-14,16-19</sup> A potential solution to these obstacles in preparing molecules with large  $S$  values and enhanced SMM properties is the discovery of new synthetic avenues to 3d compounds with exclusively ferromagnetic couplers.

<sup>a</sup>Department of Chemistry, Texas A&M University, College Station, Texas 77843, USA. E-mail: dunbar@chem.tamu.edu

<sup>b</sup>Department of Chemistry, Brock University, 1812 Sir Isaac Brock Way, L2S 3A1 St. Catharines, Ontario, Canada. E-mail: tstatamatatos@brocku.ca

† Electronic supplementary information (ESI) available: Spectroscopy data, crystallographic data and tables, and magnetism details. CCDC 1850963. For ESI and crystallographic data in CIF or other electronic format see DOI: 10.1039/c8sc04384a

Apart from their coordination versatility and multifunctional binding affinity to 3d metal ions, end-on (EO) bridging azides ( $\text{N}_3^-$ ) are also known for their ability to promote ferromagnetic exchange interactions for a wide range of M–N–M angles.<sup>20</sup> We recently demonstrated that  $\text{Me}_3\text{SiN}_3$  can be used for the synthesis of azido-bridged metal complexes without requiring the presence of any chelating or bridging organic ligand. Iso-skeletal and ferromagnetically coupled  $\{\text{Co}_7^{\text{II}}\}$  and  $\{\text{Ni}_7^{\text{II}}\}$  complexes with appreciable *S* values were obtained albeit with modest or negligible SMM properties.<sup>21</sup> Initial attempts to prepare the  $\{\text{Fe}_7^{\text{II}}\}$  analogue of this family of complexes were hampered by the prompt oxidation of  $\text{Fe}^{\text{II}}$  to  $\text{Fe}^{\text{III}}$  which led to a mixed-valence  $\{\text{Fe}^{\text{III/IIII}}\}$  2-D polymer that exhibited long-range ferromagnetic ordering below 80 K.<sup>21</sup>

Herein we report the anaerobic reaction between divalent  $\text{Fe}(\text{ClO}_4)_2 \cdot x\text{H}_2\text{O}$ ,  $\text{Me}_3\text{SiN}_3$  and  $\text{NEt}_3$  in a 1 : 4 : 1 ratio in dry MeCN to yield yellow crystals of the heptanuclear complex  $[\text{Fe}_7^{\text{II}}(\text{N}_3)_{12}(\text{MeCN})_{12}](\text{ClO}_4)_2 \cdot 4\text{MeCN}$  (**1**) in 45% yield. Complex **1**, along with the isoskeletal  $\{\text{Co}_7^{\text{II}}\}$  and  $\{\text{Ni}_7^{\text{II}}\}$  analogues,<sup>21</sup> are the first metal complexes in moderate oxidation states that are exclusively bridged by  $\text{N}_3^-$  groups without organic bridging or chelating ligands.

## Experimental section

### Synthesis

All manipulations were carried out under an inert atmosphere of  $\text{N}_2$  using standard Schlenk and glovebox techniques unless otherwise noted. The starting materials  $\text{Fe}(\text{ClO}_4)_2 \cdot x\text{H}_2\text{O}$  and  $\text{Me}_3\text{SiN}_3$  were purchased from Sigma Aldrich and used as received. The solvents MeCN and  $\text{Et}_2\text{O}$  were purchased from Sigma Aldrich, purified using an MBRAUN solvent purification system, and stored over fresh molecular sieves in an inert atmosphere prior to use. **Caution!** Azide and perchlorate salts and their corresponding metal complexes are potentially explosive; such compounds should be synthesized and used in small quantities and treated with the utmost of care at all times. Complex **1**, both in its dried (**1-d**) and as-prepared wet (**1-w**) forms, has been found to be safe when used in small quantities and under the reported conditions.

#### $[\text{Fe}_7(\text{N}_3)_{12}(\text{MeCN})_{12}](\text{ClO}_4)_2$ (**1**)

To a stirred, colorless solution of  $\text{Me}_3\text{SiN}_3$  (0.56 mL, 0.40 mmol) and  $\text{NEt}_3$  (14  $\mu\text{L}$ , 0.10 mmol) in MeCN (10 mL) was added a solution of  $\text{Fe}(\text{ClO}_4)_2 \cdot x\text{H}_2\text{O}$  (0.10 mmol, 0.04 g for  $x \sim 6$ ) in the same solvent (10 mL). The resulting purple solution was stirred for 10 min during which time a color change to dark red was observed. The solution was filtered and the filtrate was layered with  $\text{Et}_2\text{O}$  (20 mL). Orange crystals of **1**·4MeCN were obtained after 24 h. The yield was ~55%.

### Single-crystal X-ray crystallography

A single crystal of **1**·4MeCN (0.73 × 0.33 × 0.26 mm) was placed in Paratone® oil and selected under ambient conditions using a MiTeGen microloop. The crystal was placed under a stream of cold  $\text{N}_2$  at 100(1) K on a Bruker D8-QUEST diffractometer

equipped with a  $\text{I}\mu\text{S}$  Mo microsource ( $\lambda = 0.71073 \text{ \AA}$ ). An initial unit cell was determined using SAINT from a set of three  $\omega$ -scans consisting of thirty  $0.5^\circ$  frames and a sweep width of  $15^\circ$ . From this unit cell, a data collection strategy to collect all independent reflections to a resolution of at least  $0.82 \text{ \AA}$  was implemented using APEX3.<sup>22</sup>

The data for **1**·4MeCN were corrected for absorption using SADABS-2014/5.<sup>23</sup> The space group was determined from analysis of the systematic absences and E-statistics using XPREP. The structure was solved using the intrinsic phasing routine in SHELXT.<sup>24</sup> Non-hydrogen atoms were located from the Fourier difference map and refined using a least-squares refinement algorithm in SHELXL-2014<sup>25</sup> and were refined anisotropically. All hydrogen atoms were placed in calculated positions and refined with thermal parameters constrained to their parent atoms. The programs used for molecular graphics were Mercury and Diamond.<sup>26</sup> Unit cell parameters, structure solution and refinement details for **1**·4MeCN are summarized in Table S1.† Further crystallographic details can be found in the corresponding CIF file provided in the ESI.†

Compound  $[\text{Fe}_7(\text{N}_3)_{12}(\text{MeCN})_{12}](\text{ClO}_4)_2 \cdot 4\text{MeCN}$  (**1**) crystallizes in the triclinic space group  $P\bar{1}$  with one-half of the heptanuclear cation, one perchlorate anion and two MeCN molecules of crystallization in the asymmetric unit. The perchlorate anion atoms O1, O2, O3, O4 are positionally disordered over two nearly equal positions (major component occupancy: 50.6(1)%). Bond distance and thermal parameter restraints were used to model the disorder to ensure a chemically reasonable and computationally stable refinement.

## Results and discussion

### Synthesis

Crystals of  $[\text{Fe}_7^{\text{II}}(\text{N}_3)_{12}(\text{MeCN})_{12}](\text{ClO}_4)_2 \cdot 4\text{MeCN}$  were treated in two ways for the performance of magnetic and spectroscopic studies. A portion of the crystalline material was collected by filtration and dried under  $\text{N}_2$  for a maximum of 3 h (**1-d**), while the other portion of the crystalline material was immediately transferred (as-prepared) and sealed in an NMR tube (**1-w**). Selected IR data for **1-w** (Nujol mull,  $\text{cm}^{-1}$ ): 2308 (s), 2279 (s), 2103 (vs), 1459 (m), 1376 (s), 1349 (m), 1294 (m), 1260 (w), 1227 (m), 1100 (s), 1035 (w), 935 (w), 722 (m), 667 (m), 625 (s), 597 (w). For **1-d**, we were not able to perform single crystal or powder X-ray diffraction studies due to the poor crystallinity and extreme air and moisture sensitivity of the sample. Elemental analysis data of **1-d**, however, are consistent with the formula  $\{\text{Fe}_7(\text{N}_3)_{12}(\text{MeCN})_2(\text{ClO}_4)_2\}$  that accounts for the presence of the  $\{\text{Fe}_7(\text{N}_3)_{12}\}^{2+}$  core, two  $\text{ClO}_4^-$  anions and only two MeCN molecules, instead of the sixteen that appear in the crystal structure of **1** (including the interstitial MeCN molecules). Elemental analysis data for **1-d** (after drying for 3 h under  $\text{N}_2$ ), calculated for  $\text{C}_4\text{H}_6\text{N}_{38}\text{O}_8\text{Cl}_2\text{Fe}_7$ : C, 4.08; H, 0.51; N, 45.25%. Found: C, 3.95; H, 0.32; N, 45.38%. Selected IR data for **1-d** (Nujol mull,  $\text{cm}^{-1}$ ): 2104 (vs), 1635 (w), 1461 (m), 1377 (s), 1292 (m), 1225 (w), 1100 (s), 1031 (m), 914 (w), 722 (m), 666 (w), 622 (m).



The IR spectra of both **1-w** and **1-d** are depicted in Fig. S1† as a single superimposed image illustrating: (i) the presence of end-on bridging  $\text{N}_3^-$  groups (IR bands  $\sim 2100\text{ cm}^{-1}$ ),<sup>27</sup> and (ii) the de-solvation of **1** as evidenced by the disappearance of the IR bands attributed to MeCN molecules of the wet-sample ( $2280\text{--}2310\text{ cm}^{-1}$ ).<sup>28</sup> Unfortunately, the potentially explosive nature of **1** owing to the presence of a large number of azido groups as well as  $\text{ClO}_4^-$  anions, renders the use of the TGA technique impossible as an additional tool for the study of the solvation/de-solvation effects of **1**.

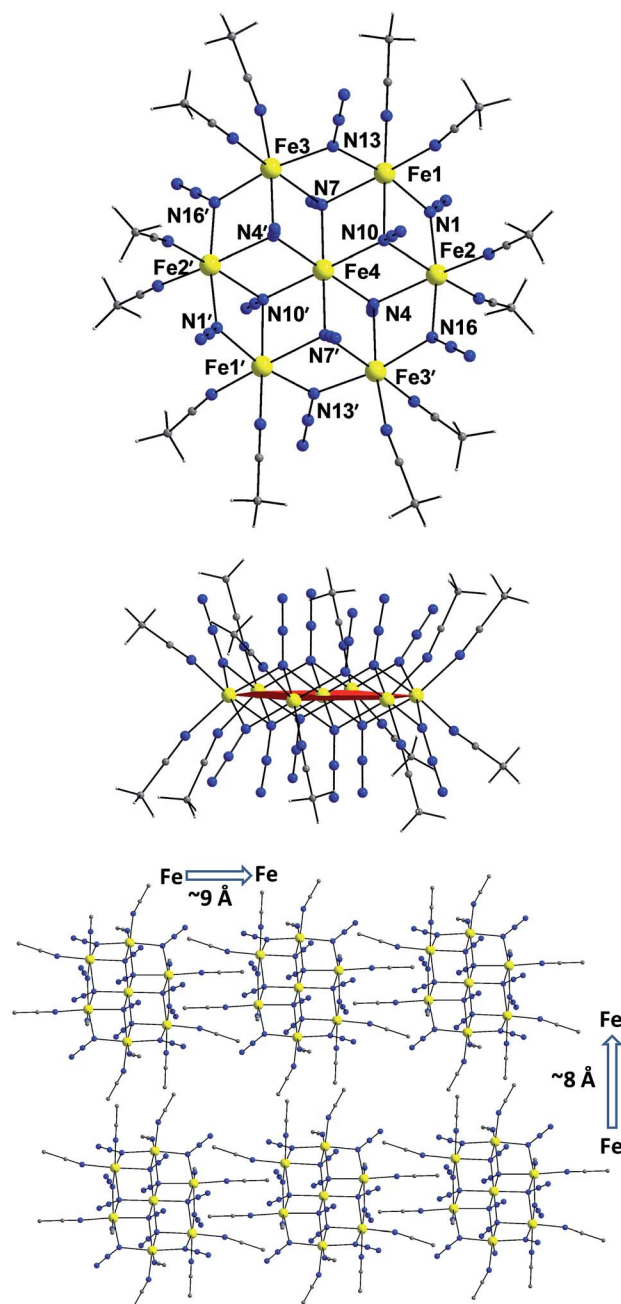
### Structural determination

The centrosymmetric heptanuclear cation in compound **1** (Fig. 1, top) consists of a nearly ideal planar hexagon of alternating  $\text{Fe}^{\text{II}}$  ions surrounding a central  $\text{Fe}^{\text{II}}$  atom, reminiscent of the known Anderson-type structure.<sup>29</sup> The oxidation states of the metal ions and the formula of **1** were determined by inspection of the metrical parameters (Table S2†), bond valence sum (BVS) calculations (Table S3†), and charge balance considerations. The  $\{\text{Fe}_7\}$  disk-like unit possesses virtual  $S_6$  symmetry and is stitched together by twelve nitrogen atoms of six  $\mu_3\text{-}1,1,1$  and six  $\mu\text{-}1,1$  end-on bridging azido ligands. The  $\mu_3\text{-}1,1,1$  azides bridge the  $\{\text{Fe}_6\}$  hexagon with the central  $\text{Fe}^{\text{II}}$  ion, while the  $\mu\text{-}1,1$  azides link the Fe centers in the outer ring to form the hexagon. Peripheral ligation is completed by twelve terminal MeCN molecules, two on each of the external  $\text{Fe}^{\text{II}}$  ions. All  $\text{Fe}^{\text{II}}$  ions are six-coordinate with nearly octahedral geometries. All of the Fe–N bond distances fall into the expected range for compounds of high-spin  $\text{Fe}^{\text{II}}$  ions with N-donor atoms.<sup>30</sup>

The  $[\text{Fe}_7(\mu_3\text{-N}_3)_6(\mu\text{-N}_3)_6]^{2+}$  inorganic core of **1** (Fig. S2†) can also be described as consisting of six  $\{\text{Fe}_3(\text{N}_3)_4\}$  partial-cubane units, each double face-sharing and which share six vertices with the central  $\text{Fe}^{\text{II}}$  ion. Complex **1** exhibits a layered structure, with layers of N atoms from azide and MeCN ligands situated above and below the  $\{\text{Fe}_7\}$  plane (Fig. 1, middle). The intra-molecular Fe...Fe separations and Fe–( $\mu\text{-N}_3$ )–Fe angles span the range  $3.336\text{--}3.354\text{ \AA}$  and  $95.6\text{--}104.9^\circ$ , respectively. Several magnetostructural correlations for azido-bridged systems, especially for  $\text{Cu}^{\text{II}}$ ,  $\text{Ni}^{\text{II}}$  and  $\text{Mn}^{\text{II}}$  complexes, have been developed and discussed in terms of the exchange interactions between non-orthogonal magnetic orbitals.<sup>20,21</sup> Importantly, the  $\text{M}^{\text{II}}\text{-N}_3(\text{EO})\text{-M}^{\text{II}}$  angles affect the nature and strength of the superexchange interactions. For divalent 3d metal complexes with EO bridging  $\text{N}_3^-$  ligands, the angle for switching from ferro- to antiferromagnetic coupling is typically  $>104^\circ$ . Exchange interactions between the  $\text{Fe}^{\text{II}}$  ions in **1** (av. Fe–N–Fe angle =  $99.2^\circ$ ) are therefore expected to be ferromagnetic on the basis of the structural parameters.<sup>19–21</sup> The packing of the  $\{\text{Fe}_7\}$  cations in the crystal (Fig. 1, bottom) lead to large separations between  $\text{Fe}^{\text{II}}$  ions of neighboring molecules, with the closest intermolecular Fe...Fe contact being  $\sim 8\text{ \AA}$  owing to the coordinated MeCN molecules.

### Magnetic susceptibility data for 1-d

Variable-temperature direct-current (DC) magnetic susceptibility measurements were initially performed on a sample of **1-**





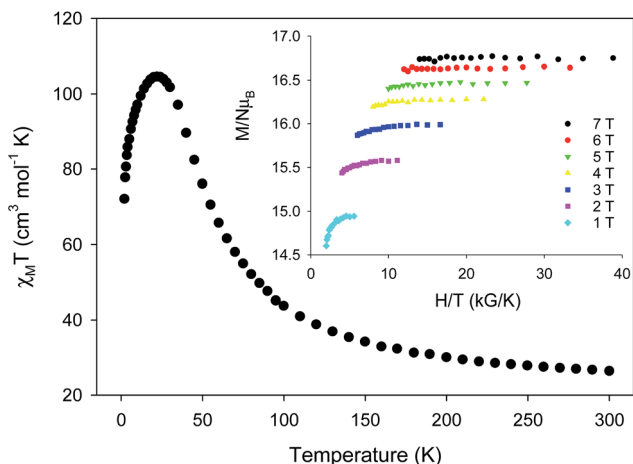


Fig. 2 Temperature dependence of  $\chi_M T$  for **1-d** at 0.1 T. (inset) Magnetization ( $M$ ) versus field ( $H$ ) and temperature ( $T$ ) data, plotted as reduced magnetization ( $M/N\mu_B$ ) versus  $H/T$ , for **1-d** at applied fields of 1–7 T and in the 1.8–5 K temperature range.

presence of significant zero-field splitting in the ground state and/or antiferromagnetic intermolecular exchange interactions between neighboring cations. The  $\chi_M T$  maximum value of  $104.61 \text{ cm}^3 \text{ mol}^{-1} \text{ K}$  at 22 K indicates an  $S = 14$  ground state, the maximum possible value for a ferromagnetically-coupled  $\{\text{Fe}_2^{\text{II}}\}$  complex; the spin-only ( $g = 2$ ) value for a state with  $S = 14$  is  $105 \text{ cm}^3 \text{ mol}^{-1} \text{ K}$ . Reduced magnetization studies performed on **1-d** at different fields and low temperatures (Fig. 2, inset) clearly indicate the presence of magnetic anisotropy as the various isofield lines do not superimpose onto a master curve expected for a system with a well-isolated spin ground state and negligible anisotropy. The magnetization curves fall substantially short of reaching the magnetization saturation of  $28 \mu_B$  expected for an  $S = 14$  ground state with  $g = 2$ , also an indication of magnetic anisotropy.

To probe the magnetization dynamics of **1-d**, alternating-current (AC) magnetic susceptibility measurements, as a function of both temperature (Fig. 3, top) and frequency (Fig. 3, middle and S3†), were performed under a zero applied dc field. Interestingly, the dried form of the  $\{\text{Fe}_2^{\text{II}}\}$  compound displays frequency dependent in-phase ( $\chi'_M$ ) and out-of-phase ( $\chi''_M$ ) signals, which are entirely resolved, at two different temperature regions. The peak maxima for **1-d** in the low- $T$  (1.8–2.6 K) and high- $T$  (2.7–5 K) regimes exhibit similar intensities (Fig. 3, inset) and they do not overlap with each other. This is indicative of two individual relaxation processes, which both appear to be thermally assisted. The data were fit to obtain relaxation times ( $\tau$ ) for the respective ac frequencies (1–933 Hz; 37 frequencies in total) and the  $T_{\text{max}}$  of the peaks (Fig. 3, inset). The data were then fit to the Arrhenius law  $[\ln \tau = \ln \tau_0 + U_{\text{eff}}/k_B T]$ , where  $U_{\text{eff}}$  is the effective energy barrier for the magnetization reversal and  $k_B$  is the Boltzmann constant, resulting in the parameters  $U_{\text{eff}} = 43.7(1) \text{ K}$  and  $\tau_0 = 4.2(1) \times 10^{-10} \text{ s}$ , and  $U_{\text{eff}} = 21.9(2) \text{ K}$  and  $\tau_0 = 1.1(2) \times 10^{-8} \text{ s}$  for the high- and low temperature regimes, respectively (Fig. 3, bottom). The pre-exponential factor,  $\tau_0$ , is usually within the  $10^{-6}$  to  $10^{-10} \text{ s}$  range for SMMs and it

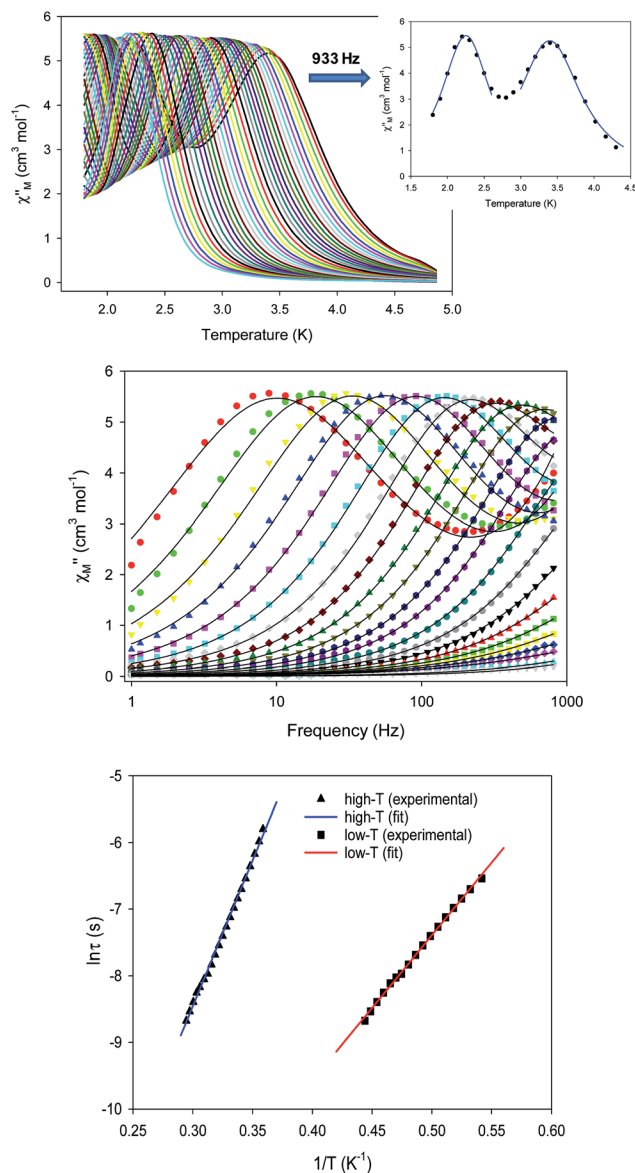


Fig. 3 (top) Out-of-phase ( $\chi''_M$ ) ac magnetic susceptibility signals for **1-d** at zero dc field. (inset)  $\chi''_M$  versus  $T$  plot at a representative ac frequency of 933 Hz showing the two separate relaxation processes at two different  $T$  regions; the solid blue lines represent fits of the data. (middle) Frequency dependence of the  $\chi''_M$  component at different temperatures (2.5–5.0 K) for **1-d** at zero dc field; the solid lines are the best fits to the generalized Debye model. (bottom) Arrhenius plot of the relaxation times ( $\tau$ ) for **1-d**; the blue and red lines correspond to the fit of the high- and low- $T$  regions, respectively.

provides a quantitative measure of the attempt time of relaxation from the thermal phonon bath.

The Cole-Cole plots (Fig. S4†) of **1-d** exhibit two sets of semicircular shapes at different temperatures; the data were fit using a generalized Debye model.<sup>31</sup> The  $\alpha$ -values for each set of low- and high-temperature data are in the range 0.26–0.38 and 0.13–0.39, respectively, suggesting the presence of multiple relaxation processes. The same magnetic results were reproduced three times from independent samples of **1** that were dried under the same conditions. The presence of two



thermally-assisted relaxation processes is a rare phenomenon in polynuclear 3d-metal SMMs and, to the best of our knowledge, has only been previously observed for a few members of the  $\{\text{Mn}_{12}\}$  family of SMMs as a result of the 'Jahn-Teller isomerism' effect.<sup>32</sup>

### Magnetic susceptibility data for 1-w

The unusual emergence of two distinct relaxation processes in **1-d** prompted us to investigate the magnetic properties of the wet (as-prepared) crystalline form of **1-w** to measure a sample in which the coordinated and interstitial MeCN molecules are intact. The freshly prepared crystalline sample of **1-w** was immediately transferred and sealed in an NMR tube which was immediately used for the acquisition of the reported magnetic data. DC magnetic susceptibility studies for **1-w**, including  $\chi_{\text{M}}T$  versus  $T$  (Fig. S5†) and reduced magnetization (Fig. S6†) studies, revealed a response similar to **1-d** and an  $S = 14$  ground state. The only noticeable difference is the decrease of the  $\chi_{\text{M}}T$  product at a lower temperature of 10 K as compared to **1-d**.

AC magnetic susceptibility studies as a function of both temperature (Fig. 4, top) and frequency (Fig. 4, middle) carried out for **1-w** led to the observation of a single slow relaxation of the magnetization below  $\sim 3$  K. The  $\chi_{\text{M}}''$  versus frequency data were fit to a generalized Debye model to extract the corresponding relaxation times. The data were then fit to the Arrhenius law (Fig. 4, bottom), yielding the parameters:  $U_{\text{eff}} = 14.1(2)$  K and  $\tau_0 = 3.3(2) \times 10^{-7}$  s. Cole-Cole plots of **1-w** exhibit semicircular shapes at different temperatures below 3 K and the fit of the data gave  $\alpha$ -values in the 0.12–0.37 range, indicating a wide distribution of relaxation times (Fig. S7†). The magnetic results of **1-w** are also reproducible, and the measurements were performed with two different wet samples of **1**. In addition, the AC magnetic dynamics of both **1-d** and **1-w** were also studied under an applied DC field of 0.1 T, but no noticeable differences were observed regarding the number of relaxation processes and magnitude of energy barriers.

### Computational studies

The experimental magnetic susceptibility data for **1** were not fit due to the large size and low symmetry of the complex. Thus, the exchange interactions and magnetic anisotropy of **1** were determined using DFT calculations in order to evaluate the observed magnetic behavior. This strategy has been previously employed in a family of  $\{\text{Mn}_7\}$  disk-like complexes, where the metal ions were bridged by organic groups, and it was able to reproduce very accurately the experimental findings.<sup>35c</sup> The exchange topology used for the computational calculations for **1** is shown in Fig. 5 (left). The following exchange Hamiltonian was employed to evaluate the magnetic exchange interactions ( $J$ ) in **1**.

$$\begin{aligned} \hat{H} = & -[2J_1(S_{\text{Fe}1}S_{\text{Fe}2} + S_{\text{Fe}1}S_{\text{Fe}3} + S_{\text{Fe}1}S_{\text{Fe}4} + S_{\text{Fe}1}S_{\text{Fe}5} \\ & + S_{\text{Fe}1}S_{\text{Fe}6} + S_{\text{Fe}1}S_{\text{Fe}7}) + 2J_2(S_{\text{Fe}2}S_{\text{Fe}3} + S_{\text{Fe}3}S_{\text{Fe}4} \\ & + S_{\text{Fe}4}S_{\text{Fe}5} + S_{\text{Fe}5}S_{\text{Fe}6} + S_{\text{Fe}6}S_{\text{Fe}7} + S_{\text{Fe}2}S_{\text{Fe}7})] \end{aligned} \quad (1)$$

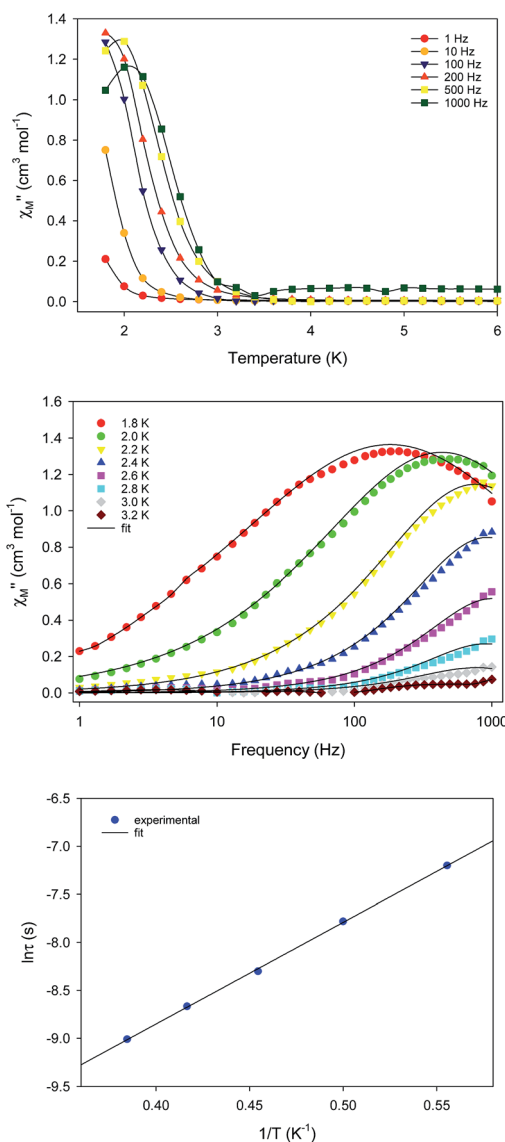


Fig. 4 (top) Out-of-phase ( $\chi_{\text{M}}''$ ) ac magnetic susceptibility signals for **1-w** at zero dc field; the solid lines are guides for the eye. (middle) Frequency dependence of  $\chi_{\text{M}}''$  at different temperatures for **1-w** at zero dc field; the solid lines are best fits to the generalized Debye model. (bottom) Arrhenius plot of  $\tau$  versus  $1/T$  for **1-w**; the solid line is the best fit as described in the text.

To extract the exchange interactions on the full structure of **1**, the energies of three different spin configurations were used (Table S4†).<sup>33</sup> The exchange coupling constants were calculated using the broken symmetry (BS) approach developed by Noodleman.<sup>34</sup> This method has been employed extensively to compute good numerical estimates of exchange interactions in numerous polynuclear complexes.<sup>35</sup> DFT calculations were performed using the B3LYP basis functional<sup>36</sup> and Aldrich's triple- $\zeta$ -quality basis set<sup>37</sup> with the Gaussian 09 program.<sup>38</sup>

Apart from the magnetic coupling, the ZFS ( $D$ ) has also been computed for complex **1** using the Orca 3.0 programme suite.<sup>39</sup> In our DFT calculations, the spin-orbit coupling operators are represented by an effective one electron, using the spin-orbit mean field (SOMF) method as implemented in Orca.<sup>39</sup> We have



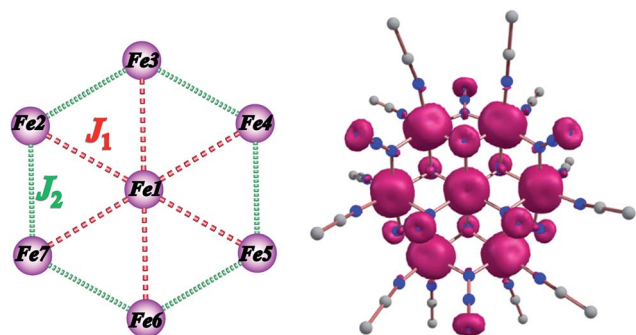


Fig. 5 (left) Magnetic exchange pathways in complex **1**; see the text for the DFT computed values. (right) DFT-computed spin-density plots for **1** for which all spins are up, rationalizing the experimental  $S = 14$  ground state. The pink and blue colours represent positive and negative spin densities, respectively.

used the coupled perturbed (CP) SOC approach to evaluate the spin-orbit contribution to  $D$  ( $D_{\text{SOC}}$ ). The spin-spin contribution ( $D_{\text{SS}}$ ) was estimated by using the unrestricted natural orbital<sup>40</sup> approach. Furthermore, to improve the accuracy of the estimated  $D$  values, relativistic corrections are performed using the DKH method.<sup>39</sup>

The coupling between the central and the outer  $\text{Fe}^{\text{II}}$  ions is designated as the  $J_1$  interaction and the coupling between the two outer ring  $\text{Fe}^{\text{II}}$  ions is described as  $J_2$  interaction. The DFT computed values predict that both the  $J_1$  and  $J_2$  interactions are ferromagnetic with values of  $+3.0$  and  $+3.3 \text{ cm}^{-1}$ , respectively. Ferromagnetic coupling is consistent with the observation of ferromagnetic interactions in dinuclear  $\text{Ni}(\text{II})$ ,  $\text{Fe}(\text{III})$  and  $\text{Mn}(\text{II})$  complexes with one or more  $\mu$ -bridging azido ligands<sup>41</sup> and in the azido-bridged  $\{\text{Ni}_7\}$  and  $\{\text{Co}_7\}$  disk-like complexes.<sup>21</sup> Given that both  $J_1$  and  $J_2$  interactions are ferromagnetic, the ground state is  $S = 14$ . The computed spin density plots (Fig. 5, right) reveal a dominant spin delocalization mechanism. Calculations were performed also by using the diamagnetic substitution method (DSM), where, except for the desired pair of  $\text{Fe}^{\text{II}}$  centres, the remaining ions are substituted by diamagnetic  $\text{Zn}^{\text{II}}$  ions.<sup>35c,42</sup> Such calculations are essential for validating the  $J$  values computed from the full structure and to realize the influence of other paramagnetic centres on a particular  $J$  value. This method also yields ferromagnetic coupling constants for both interactions ( $J_1 = +3.1$  and  $J_2 = +4.5 \text{ cm}^{-1}$ ) which are in excellent agreement with the full cluster coupling values.

Given the large ground state spin value and the observed slow relaxation of the magnetization for **1** at zero DC field, one would expect a negative  $D$  value for the molecule, thus the value of  $D$  was computed to further probe the SMM behavior. Although *ab initio* CASSCF/NEVPT2 calculations have proven to yield accurate estimates of  $D$  values,<sup>43</sup> this method cannot be employed for such large molecules.<sup>44</sup> The full cluster anisotropy was therefore computed using DFT methods which yielded the parameters  $D = -0.2323 \text{ cm}^{-1}$  and  $E/D = 0.027$ , where  $E$  is the rhombic zero-field splitting parameter. The  $D_{\text{SOC}}$  plays a key role with a value of  $-0.191 \text{ cm}^{-1}$ . The major contributions to  $D_{\text{SOC}}$  arise from DOMO (doubly-occupied molecular orbital) to SOMO (singly-occupied MO)  $\beta \rightarrow \beta$  excitations ( $-0.127 \text{ cm}^{-1}$ ) and

SOMO to SOMO  $\alpha \rightarrow \beta$  excitations ( $-0.072 \text{ cm}^{-1}$ ). The SOMO to VMO (Virtual Molecular Orbital)  $\alpha \rightarrow \alpha$  excitations and DOMO to VMO  $\beta \rightarrow \alpha$  excitations contribute to a small extent with values of  $0.003$  and  $0.005 \text{ cm}^{-1}$ , respectively.<sup>45</sup> Comparable behavior is observed for  $D_{\text{SS}}$  contributions of  $-0.04 \text{ cm}^{-1}$ .

### Magnetic properties of 1-d versus 1-w

The differences in the magnetic properties of **1-d** versus **1-w**, as indicated by the low temperature regimes of the  $\chi_{\text{M}}T$  versus  $T$  plots and the AC magnetic susceptibility data, are due, in part, to the changes in intermolecular interactions between the individual  $\{\text{Fe}_7^{\text{II}}\}$  molecules. The intermolecular distances in **1-w** are expected to be larger due to the presence of all of the MeCN ligands (Fig. 1, bottom). In the case of **1-d**, the drying process results in the removal of MeCN molecules and the  $\{\text{Fe}_7^{\text{II}}\}$  cations are expected to be less well separated in the solid state. Moreover, the molecular magnetic anisotropy of **1** is expected to deviate from **1-w** to **1-d** due to the dissimilar coordination environment of the six peripheral  $\text{Fe}^{\text{II}}$  ions. In **1-w**, all of the  $\text{Fe}^{\text{II}}$  ions are six-coordinate with a distorted octahedral geometry. In **1-d**, however, drying leads to loss of coordinated MeCN molecules and the peripheral  $\text{Fe}^{\text{II}}$  ions will be primarily four-coordinate. These low-coordinate  $\text{Fe}^{\text{II}}$  ions are expected to exhibit larger single-ion magnetic anisotropies which, in turn, effects the global molecular anisotropy.<sup>46</sup> For example, complete removal of all twelve bound MeCN molecules in **1** would render the six external  $\text{Fe}^{\text{II}}$  ions four-coordinate with slightly distorted see-saw geometries (CShM values =  $0.82$ – $0.85$ ,  $C_{2v}$  point group; Fig. S8 and Table S5†). In support of this contention is the fact that large uniaxial magnetic anisotropy and slow magnetization relaxation with high energy barriers have been reported for a family of four-coordinate, trigonal pyramidal  $\text{Fe}^{\text{II}}$ –pyrrolide complexes with  $C_{3v}$  point group symmetry.<sup>47</sup> Therefore, the crystal field around four-coordinate  $\text{Fe}^{\text{II}}$  ions in **1-d** would induce increased molecular magnetic anisotropy for this system and consequently a larger energy barrier than for **1-w**. It is also possible that the two  $\text{ClO}_4^-$  anions found in the elemental analyses of **1-d** are bound to the  $\text{Fe}^{\text{II}}$  centers. Although rare,<sup>48a-c</sup> terminally coordinated  $\text{ClO}_4^-$  ions are of precedence in  $\text{Fe}^{\text{II}}$  chemistry, and this is also expected to affect the crystal field and coordination geometries of some of the outer  $\text{Fe}^{\text{II}}$  ions in **1-d**. On a final note, the shift ( $\Delta T_{\text{max}}$ ) in the  $\chi''_{\text{M}}$  peak maximum temperature ( $T_{\text{max}}$ ) with AC frequency ( $f$ ) was measured by a parameter  $\phi = (\Delta T_{\text{max}}/T_{\text{max}})/\Delta(\log f)$ . For the dried sample, **1-d**, we obtained  $\phi = 0.11$ – $0.19$  and  $0.17$ – $0.22$  for the high- and low- $T$  regions, which are both within the range of normal superparamagnets, thereby excluding the possibility of a spin glass state.<sup>48d</sup>

## Conclusions and outlook

In summary, the synthesis of a rare, ferromagnetically-coupled  $\{\text{Fe}_7^{\text{II}}\}$  (**1**) disk-like cluster with an  $S = 14$  ground state and unusual “Janus”-faced SMM behavior has been found to exhibit different AC magnetic dynamics in the dried (**1-d**) versus wet (**1-w**) forms of the crystals. Such a rare phenomenon in 3d-cluster





SMs is primarily rationalized in terms of the loss or presence of coordinated/interstitial MeCN molecules in **1-d** or **1-w**, respectively. The  $[\text{Fe}_7(\text{N}_3)_{12}]^{2+}$  core is present in both forms of **1**, as confirmed by X-ray diffraction studies (for **1-w**), elemental analyses (for **1-d**) and DC magnetic studies ( $S = 14$  for both forms). The different number of relaxation processes (two for **1-d** and one for **1-w**) and values of energy barriers for the magnetization reversal are attributed to differences in intermolecular interactions<sup>49</sup> and the dissimilar molecular anisotropies emanating from different crystal fields around the peripheral  $\text{Fe}^{\text{II}}$  ions.

These results underscore the importance of solvation/desolvation effects on the structural and magnetic properties of polynuclear metal complexes and the sensitivity of magnetic dynamics upon altering the first coordination sphere of 3d-metal ions.

## Conflicts of interest

There are no conflicts to declare.

## Acknowledgements

K. R. D. gratefully acknowledges support for this work by the National Science Foundation (CHE-1808779) and the Robert A. Welch Foundation (Grant A-1449). The SQUID magnetometer was purchased with funds provided by the Texas A&M University Vice President of Research. We are grateful to the HPRC at Texas A&M for the computing resources. Th. C. S. thanks NSERC-DG, ERA and Brock Chancellor's Chair for Research Excellence.

## Notes and references

- R. Bagai and G. Christou, *Chem. Soc. Rev.*, 2009, **38**, 1011–1026.
- M. del Carmen Giménez-López, F. Moro, A. La Torre, C. J. Gómez-García, P. D. Brown, J. van Slageren and A. N. Khlobystov, *Nat. Commun.*, 2011, **2**, 407.
- R. Vincent, S. Klyatskaya, M. Ruben, W. Wernsdorfer and F. Balestro, *Nature*, 2012, **488**, 357.
- G. Aromi, D. Aguila, P. Gamez, F. Luis and O. Roubeau, *Chem. Soc. Rev.*, 2012, **41**, 537–546.
- P. W. Anderson, *Phys. Rev.*, 1950, **79**, 350–356.
- S. Demir, I.-R. Jeon, J. R. Long and T. D. Harris, *Coord. Chem. Rev.*, 2015, **289–290**, 149–176.
- D. Gatteschi and L. Sorace, *J. Sol. State Chem.*, 2001, **159**, 253–261.
- J. D. Rinehart and J. R. Long, *Chem. Sci.*, 2011, **2**, 2078–2085.
- D. N. Woodruff, R. E. P. Winpenny and R. A. Layfield, *Chem. Rev.*, 2013, **113**, 5110–5148.
- K. Binnemans, *Chem. Rev.*, 2009, **109**, 4283–4374.
- (a) J. M. Frost, K. L. M. Harriman and M. Murugesu, *Chem. Sci.*, 2016, **7**, 2470–2491; (b) C. Papatriantafyllopoulou, E. E. Moushi, G. Christou and A. J. Tasiopoulos, *Chem. Soc. Rev.*, 2016, **45**, 1597–1628.
- N. E. Chakov, S.-C. Lee, A. G. Harter, P. L. Kuhns, A. P. Reyes, S. O. Hill, N. S. Dalal, W. Wernsdorfer, K. A. Abboud and G. Christou, *J. Am. Chem. Soc.*, 2006, **128**, 6975–6989.
- C. J. Milios, A. Vinslava, W. Wernsdorfer, S. Moggach, S. Parsons, S. P. Perlepes, G. Christou and E. K. Brechin, *J. Am. Chem. Soc.*, 2007, **129**, 2754–2755.
- P. Abbasi, K. Quinn, D. I. Alexandropoulos, M. Damjanović, W. Wernsdorfer, A. Escuer, J. Mayans, M. Pilkington and T. C. Stamatatos, *J. Am. Chem. Soc.*, 2017, **139**, 15644–15647.
- K. Chakarawet, P. C. Bunting and J. R. Long, *J. Am. Chem. Soc.*, 2018, **140**, 2058–2061.
- C. J. Milios and R. E. P. Winpenny, in *Molecular Nanomagnets and Related Phenomena*, ed. S. Gao, Springer Berlin Heidelberg, Berlin, Heidelberg, 2015, pp. 1–109.
- A. K. Boudalis, Y. Sanakis, J. M. Clemente-Juan, A. Mari and J. P. Tuchagues, *Eur. J. Inorg. Chem.*, 2007, 2409–2415.
- H. Oshio, N. Hoshino, T. Ito and M. Nakano, *J. Am. Chem. Soc.*, 2004, **126**, 8805–8812.
- A. K. Boudalis, Y. Sanakis, J. M. Clemente-Juan, B. Donnadieu, V. Nastopoulos, A. Mari, Y. Coppel, J. P. Tuchagues and S. P. Perlepes, *Chem.-Eur. J.*, 2008, **14**, 2514–2526.
- A. Escuer, J. Esteban, S. P. Perlepes and T. C. Stamatatos, *Coord. Chem. Rev.*, 2014, **275**, 87–129.
- D. I. Alexandropoulos, L. Cunha-Silva, A. Escuer and T. C. Stamatatos, *Chem.-Eur. J.*, 2014, **20**, 13860–13864.
- APEX-III, Bruker AXS Inc, Data Collection Software, Bruker AXS, Delft, USA, 2016.
- G. M. Sheldrick, *SADABS v.2.01*, Bruker/Siemens Area Detector Absorption Correction Program, Bruker AXS, Madison, WI, 1998.
- G. M. Sheldrick, *Acta Crystallogr. Sect. A, Found. and Adv.*, 2015, **71**, 3–8.
- G. M. Sheldrick, *Acta Crystallogr., Sect. C: Struct. Chem.*, 2015, **71**, 3–8.
- (a) C. F. Macrae, P. R. Edgington, P. McCabe, E. Pidcock, G. P. Shields, R. Taylor, M. Towler and J. van de Streek, *J. Appl. Crystallogr.*, 2006, **39**, 453–457; (b) W. Pennington, *J. Appl. Crystallogr.*, 1999, **32**, 1028–1029.
- T. C. Stamatatos, G. S. Papaefstathiou, L. R. MacGillivray, A. E. Escuer, R. Vicente, E. Ruiz and S. P. Perlepes, *Inorg. Chem.*, 2007, **46**, 8843.
- K. Nakamoto, *Infrared and Raman Spectra of Inorganic and Coordination Compounds*, 4th edn, Wiley, New York, 1986.
- N. Hoshino, A. M. Ako, A. K. Powell and H. Oshio, *Inorg. Chem.*, 2009, **48**, 3396–3407.
- H. Phan, J. J. Hrudka, D. Igimbayeva, L. M. Lawson Daku and M. Shatruk, *J. Am. Chem. Soc.*, 2017, **139**, 6437–6447.
- K. S. Cole and R. H. Cole, *J. Chem. Phys.*, 1941, **9**, 341–351.
- S. M. J. Aubin, Z. Sun, H. J. Eppley, E. M. Rumberger, I. A. Guzei, K. Folting, P. K. Gantzel, A. L. Rheingold, G. Christou and D. N. Hendrickson, *Inorg. Chem.*, 2001, **40**, 2127–2146.
- A. Bencini and F. Totti, *Int. J. Quantum Chem.*, 2005, **101**, 819–825.
- L. Noodleman, *J. Am. Chem. Soc.*, 1981, **74**, 5737–5743.



- 35 (a) P. Christian, G. Rajaraman, A. Harrison, J. J. W. McDouall, J. T. Raftery and R. E. P. Winpenny, *Dalton Trans.*, 2004, 1511–1512; (b) G. Rajaraman, E. Ruiz, J. Cano and S. Alvarez, *Chem. Phys. Lett.*, 2005, **415**, 6–9; (c) K. R. Vignesh, S. K. Langley, K. S. Murray and G. Rajaraman, *Chem.–Eur. J.*, 2015, **21**, 2881–2892.
- 36 A. D. Becke, *J. Chem. Phys.*, 1993, **98**, 5648–5652.
- 37 A. Schäfer, C. Huber and R. Ahlrichs, *J. Chem. Phys.*, 1994, **100**, 5829–5835.
- 38 M. J. Frisch, G. W. Trucks, H. B. Schlegel, G. E. Scuseria, M. A. Robb, J. R. Cheeseman, G. Scalmani, V. Barone, B. Mennucci, G. A. Petersson, H. Nakatsuji, M. Caricato, X. Li, H. P. Hratchian, A. F. Izmaylov, J. Bloino, G. Zheng, J. L. Sonnenberg, M. Hada, M. Ehara, K. Toyota, R. Fukuda, J. Hasegawa, M. Ishida, T. Nakajima, Y. Honda, O. Kitao, H. Nakai, T. Vreven, J. A. Montgomery, J. E. P. Jr, F. Ogliaro, M. Bearpark, J. J. Heyd, E. Brothers, K. N. Kudin, V. N. Staroverov, R. Kobayashi, J. Normand, K. Raghavachari, A. Rendell, J. C. Burant, S. S. Iyengar, J. Tomasi, M. Cossi, N. Rega, J. M. Millam, M. Klene, J. E. Knox, J. B. Cross, V. Bakken, C. Adamo, J. Jaramillo, R. Gomperts, R. E. Stratmann, O. Yazyev, A. J. Austin, R. Cammi, C. Pomelli, J. W. Ochterski, R. L. Martin, K. Morokuma, V. G. Zakrzewski, G. A. Voth, P. Salvador, J. J. Dannenberg, S. Dapprich, A. D. Daniels, Ö. Farkas, J. B. Foresman, J. V. Ortiz, a. J. Cioslowski, D. J. Fox and I. Gaussian, *Revision A.02 ed., Gaussian 09*, Wallingford CT, 2009.
- 39 F. Neese, *Wiley Interdiscip. Rev.: Comput. Mol. Sci.*, 2012, **2**, 73–78.
- 40 K. Koizumi, M. Shoji, Y. Kitagawa, T. Taniguchi, T. Kawakami, M. Okumura and K. Yamaguchi, *Polyhedron*, 2005, **24**, 2720–2725.
- 41 (a) R. Cortes, J. L. Pizarro, L. Lezama, M. I. Arriortua and T. Rojo, *Inorg. Chem.*, 1994, **33**, 2697–2700; (b) G. De Munno, T. Poerio, G. Viau, M. Julve and F. Lloret, *Angew. Chem., Int. Ed.*, 1997, **36**, 1459–1461; (c) J. Ribas, M. Monfort, C. Diaz, C. Bastos and X. Solans, *Inorg. Chem.*, 1994, **33**, 484–489.
- 42 E. Ruiz, J. Cano, S. Alvarez, A. Caneschi and D. Gatteschi, *J. Am. Chem. Soc.*, 2003, **125**, 6791–6794.
- 43 (a) S. Sinnecker, F. Neese, L. Noodleman and W. Lubitz, *J. Am. Chem. Soc.*, 2004, **126**, 2613–2622; (b) S. K. Singh and G. Rajaraman, *Chem.–Eur. J.*, 2014, **20**, 113–123.
- 44 K. R. Vignesh, S. K. Langley, C. J. Gartshore, B. Moubaraki, K. S. Murray and G. Rajaraman, *Inorg. Chem.*, 2017, **56**, 1932–1949.
- 45 M. Schmidt, D. Wiedemann, B. Moubaraki, N. F. Chilton, K. S. Murray, K. R. Vignesh, G. Rajaraman and A. Grohmann, *Eur. J. Inorg. Chem.*, 2013, 958–967.
- 46 (a) R. Maurice, P. Verma, J. M. Zadrozny, S. Luo, J. Borycz, J. R. Long, D. G. Truhlar and L. Gagliardi, *Inorg. Chem.*, 2013, **52**, 9379–9389; (b) M. Atanasov, J. M. Zadrozny, J. R. Long and F. Neese, *Chem. Sci.*, 2013, **4**, 139–156; (c) J. M. Zadrozny, D. J. Xiao, M. Atanasov, G. J. Long, F. Grandjean, F. Neese and J. R. Long, *Nat. Chem.*, 2013, **5**, 577; (d) J. M. Zadrozny, M. Atanasov, A. M. Bryan, C.-Y. Lin, B. D. Reken, P. P. Power, F. Neese and J. R. Long, *Chem. Sci.*, 2013, **4**, 125–138.
- 47 W. H. Harman, T. D. Harris, D. E. Freedman, H. Fong, A. Chang, J. D. Rinehart, A. Ozarowski, M. T. Sougrati, F. Grandjean, G. J. Long, J. R. Long and C. J. Chang, *J. Am. Chem. Soc.*, 2010, **132**, 18115–18126.
- 48 (a) O. Singh, N. Tyagi, M. M. Olmstead and K. Ghosh, *Dalton Trans.*, 2017, **46**, 14186–14191; (b) S. K. Ghosh, R. Patra and S. P. Rath, *Inorg. Chem.*, 2010, **49**, 3449–3460; (c) K. Chen and L. Que Jr, *J. Am. Chem. Soc.*, 2001, **123**, 6327–6337; (d) J. A. Mydosh, *Spin Glasses: An Experimental Introduction*, Taylor & Francis, London, 1993.
- 49 For mononuclear 3d-SMMs exhibiting two relaxation processes, see: (a) J. M. Zadrozny and J. R. Long, *J. Am. Chem. Soc.*, 2011, **133**, 20732–20734; (b) F. Habib, O. R. Luca, V. Vieru, M. Shiddiq, I. Korobkov, S. I. Gorelsky, M. K. Takase, L. F. Chibotaru, S. Hill, R. H. Crabtree and M. Murugesu, *Angew. Chem., Int. Ed.*, 2013, **52**, 11290–11293; (c) F. Habib, I. Korobkov and M. Murugesu, *Dalton Trans.*, 2015, **44**, 6368–6373; (d) J. Miklovič, D. Valigura, R. Boča and J. Titiš, *Dalton Trans.*, 2015, **44**, 12484–12487; (e) J. Li, Y. Han, F. Cao, R.-M. Wei, Y.-Q. Zhang and Y. Song, *Dalton Trans.*, 2016, **45**, 9279–9284; (f) L. T. A. Ho and L. F. Chibotaru, *Phys. Rev. B: Condens. Matter Mater. Phys.*, 2016, **94**, 104422.

